



Cite this: *RSC Adv.*, 2017, 7, 34096

Decoration of TiO₂/g-C₃N₄ Z-scheme by carbon dots as a novel photocatalyst with improved visible-light photocatalytic performance for the degradation of enrofloxacin†

Yuehan Su,  Ping Chen, Fengliang Wang, Qianxin Zhang, Tiansheng Chen, Yingfei Wang, Kun Yao, Wenying Lv and Guoguang Liu *

A novel visible-light-driven carbon dot (CDs)/TiO₂/g-C₃N₄ photocatalyst was successfully synthesized by doping CDs in TiO₂ nanoparticles and the surface of g-C₃N₄ nanosheets via a facile hydrothermal process and was confirmed by characterization methods. UV-vis diffuse reflectance spectra (DRS) revealed that CDs/TiO₂/g-C₃N₄ showed obvious additional absorption in the 370–450 nm region. DMPO spin-trapping ESR spectra demonstrated the existence of O₂^{•−} and ·OH. The photocatalytic activity of the CDs (1.0 wt%)/TiO₂/g-C₃N₄ was remarkably enhanced as compared to that of the single components (TiO₂ and g-C₃N₄) and double component (TiO₂/g-C₃N₄) towards the degradation of enrofloxacin (ENX) under visible-light irradiation. About 91.6% of ENX was decomposed by CDs (1.0 wt%)/TiO₂/g-C₃N₄ in 1 h, which is nearly 3.95 times, 4.82 times, and 1.69 times that for TiO₂, g-C₃N₄, and TiO₂ (90.0 wt%)/g-C₃N₄, respectively. Scavenging experiments revealed that O₂^{•−} and ·OH played key roles during the photocatalytic degradation of ENX. This study provides a simple and convenient method to modify materials with enhanced photocatalytic performance, and the CDs/TiO₂/g-C₃N₄ catalyst is efficient, stable, and reusable for environmental practical applications.

Received 15th May 2017

Accepted 17th June 2017

DOI: 10.1039/c7ra05485h

rsc.li/rsc-advances

Introduction

In the past decade, use of solar-energy-driven semiconductors as photocatalysts to remove aquatic contaminants became one of the most promising approaches.^{1–3} As is known, semiconductor titanium dioxide (TiO₂) plays a significant role in the field of photocatalysis due to its nontoxicity, inexpensiveness, high activity, *etc.*⁴ However, TiO₂ has a band gap of approximately 3.2 eV, which requires ultraviolet irradiation with wavelengths less than 385 nm for activation. That is, this excitation wavelength can activate electron transfer from the TiO₂ valence band (VB) to the conduction band (CB). Consequently, the photocatalyst utilizes less than 5% of the energy available in sunlight, which extremely restricts its application in practice.^{5–7} More recently, a metal-free semiconductor, graphitic carbon nitride (g-C₃N₄), has been successfully synthesized through a facile thermal polycondensation method.^{8,9} It is reported that g-C₃N₄ exhibits high photocatalytic activity due to its delocalized conjugated π structures, leading to relatively rapid photoinduced charge separation and slow charge

recombination.¹⁰ Furthermore, the low band gap (2.70 eV) capacitates g-C₃N₄ to efficiently harvest sunlight within the visible-light region. Although g-C₃N₄ possesses better photocatalytic activity as compared to TiO₂, it is far from enough to meet the demands in practical use. Various attempts including surface sensitization, chemical modification, and coupling with other semiconductor materials have been made to increase the photocatalytic efficiency of TiO₂ and g-C₃N₄.^{9,11,12} Much interest has recently been concentrated on the fabrication of TiO₂/g-C₃N₄ heterostructures, which extend the absorption to the visible-light region.^{13–15} However, to the best of our knowledge, h⁺ from E_{VB} of g-C₃N₄ is incapable of generating ·OH under visible light; in addition to the abovementioned shortcomings of TiO₂, the photocatalytic performance of TiO₂/g-C₃N₄ is still unsatisfactory.

Carbon dots (CDs), with an appealing group of zero-dimensional nanostructures, have attracted extensive research interest in the photocatalytic field due to their low-cost, aqueous dispersibility, chemical stability, unique photoinduced electron transfer, and electron reservoir properties.¹⁶ Hence, photocatalysts with the incorporation of CDs have achieved excellent effects in the past few years. For example, Guo *et al.* synthesized a carbon quantum dot/carbon nitride hybrid photocatalyst to improve the photocatalytic degradation of methyl orange.¹⁷ Wu *et al.* used CDs as a solid-state electron mediator for the

School of Environmental Science and Engineering, Institute of Environmental Health and Pollution Control, Guangdong University of Technology, Guangzhou, 510006, China. E-mail: liugg615@163.com

† Electronic supplementary information (ESI) available. See DOI: 10.1039/c7ra05485h

preparation of BiVO₄/CD/CdS Z-scheme photocatalyst, which showed excellent photocatalytic activity and stability for overall water splitting under visible light.¹⁸ Recently, Yu *et al.* reported a novel CD/ZnFe₂O₄ composite photocatalyst with enhanced photocatalytic performance for the removal of NO_x, demonstrating that CDs acted as an electron reservoir and transporter as well as a powerful energy-transfer component.¹⁹ Due to the outstanding photocatalytic properties, in this study, CDs were first used for the decoration of the TiO₂/g-C₃N₄ Z-scheme through a facile hydrothermal-polymerized method.

Pharmaceuticals and personal care products (PPCPs), as emerging contaminants in recent years, have received unprecedented concern because of their potential hazard to the ecological environment and human health.²⁰ According to the previous study, PPCPs have been confirmed to be ubiquitous throughout the world,^{21–24} and even worse, the drinking water treatment plants are also included.^{25,26} Consequently, it is extremely urgent to develop efficient methods for the elimination of PPCPs in aquatic environments.

In this study, the visible-light-driven CD/TiO₂/g-C₃N₄ ternary composites were first synthesized and used as photocatalysts for the degradation of PPCPs. Herein, enrofloxacin (ENX), largely used as veterinary bactericides, was taken as targeted PPCPs under the effects of the as-prepared materials. The structural and optical properties of the composites were investigated in detail by TEM, XRD, XPS, PL, *etc.* In addition, the influence of the TiO₂ : g-C₃N₄ molar ratio and doping amount of CDs on the photocatalytic performance of these composite photocatalysts was studied in an attempt to illuminate the potential mechanisms. The CD/TiO₂/g-C₃N₄ ternary composites were efficient towards the decomposition of refractory pollutants because of the synergic effect of accelerated charge separation and an extended light harvesting region. It was anticipated that this study could be instrumental in studying the removal of PPCPs and fabrication of novel ternary composite photocatalysts.

Experimental

Materials

Enrofloxacin (ENX, 98% purity) was acquired from TCI Reagent Co. Ltd. (China). Degussa P25 (commercial TiO₂) was purchased from Sinopharm Chemical Reagent Co. Ltd. (Shanghai, China). Dicyandiamide was commercially purchased from Aladdin (China). Acetonitrile and methanol were obtained from CNW Technologies GmbH (Germany, HPLC-grade). Other reagents (*e.g.*, citric acid, urea, acetic acid, sulfuric acid, sodium hydroxide, benzoquinone, isopropanol, potassium iodide, and sodium azide) were of analytical grade and used without further purification. Deionized (DI) water from a Milli-Q apparatus (Germany) was used in the whole experiment.

Synthetic procedures

Preparation of the CDs. C-Dots were prepared *via* the hydrothermal method and modified according to a previous report.²⁷ Briefly, a weighed quantity (3.0 g) of citric acid and (3.0

g) urea was mixed with 10 mL DI water, which was placed into a Teflon autoclave for 5 h at 180 °C. After being cooled to room temperature, the obtained brown water solution was centrifuged at 10 000 rpm for 15 min to remove large particles. Finally, the remaining solution was transferred to the vacuum drier for 3 h at 80 °C to obtain a brownish black solid (C-dots).

Preparation of g-C₃N₄. g-C₃N₄ was prepared by directly heating dicyandiamide.²⁸ In brief, 5.0 g of dicyandiamide was placed in an alumina crucible with a cover and then heated to 550 °C for 3 h at a heating rate of 2.8 °C min^{−1}. After being cooled down to room temperature, the obtained bulk g-C₃N₄ was milled into powders for further use.

Preparation of the TiO₂/g-C₃N₄ binaries. The TiO₂/g-C₃N₄ composites were prepared using a typical method.²⁹ Briefly, an appropriate amount of TiO₂ was mixed with 20 mL of methanol in a beaker and sonicated until it was completely dispersed. After this, a calculated amount of g-C₃N₄ was mixed with the TiO₂ suspension and stirred in a fume hood for 15 h. Subsequently, the obtained materials were transferred to a muffle furnace and heated to 550 °C at a heating rate of 2.8 °C min^{−1}, and the temperature was maintained at 550 °C for 3 h. Through this method, a series of TiO₂ (wt%)/g-C₃N₄ photocatalysts (wt = 10.0, 30.0, 60.0, and 90.0) were synthesized and labelled as TCN-*x* (*x* = 10, 30, 60, and 90, respectively).

Decoration of the CDs onto TiO₂/g-C₃N₄ composites. The CDs/TiO₂/g-C₃N₄ ternary photocatalysts with different doping amounts of CDs (0.5, 1, 2, and 3 wt%) were synthesized as follows: first, the optimal mass ratio of the as-prepared TiO₂/g-C₃N₄ that exhibited the best performance for the photocatalytic degradation of ENX was placed in an alumina crucible with a cover. After this, a series of different mass ratios of CDs were added to the alumina crucible and heated to 550 °C for 3 h at a heating rate of 2.8 °C min^{−1}. After being cooled down to room temperature, the final CD/TiO₂/g-C₃N₄ composite photocatalysts were obtained and denoted as CTCN-0.5, CTCN-1, CTCN-2, and CTCN-3.

Characterization

Thermogravimetric (TG) analysis was conducted using STA-449C Jupiter (NETZSCH Corporation, Germany). The inter-layer structure of the samples was characterized by a transmission electron microscope (TEM, JEM-2100HR). The crystal structure and phase purity of the obtained materials were tested by X-ray diffraction (XRD, BRUKER D8 ADVANCE) equipped with Cu K α radiation (λ = 0.154178 nm). The UV-vis diffuse reflection spectra (DRS) of the as-prepared samples were analyzed *via* a UV2450 UV-vis spectrophotometer (Shimadzu) using BaSO₄ as a reflectance standard. X-ray photoelectron spectroscopy (XPS) was used to analyze the ionic characteristics, which was conducted using a Thermo VG ESCALAB 250 spectrometer with Al K α radiation at 1486.6 eV. Fourier transform infrared (FT-IR) spectra were obtained using a Nicolet 6700 spectrophotometer (ThermoFisher). Photoluminescence (PL) spectra were obtained using a FluoroMax-4 fluorescence spectrophotometer (HORIBA Jobin Yvon).



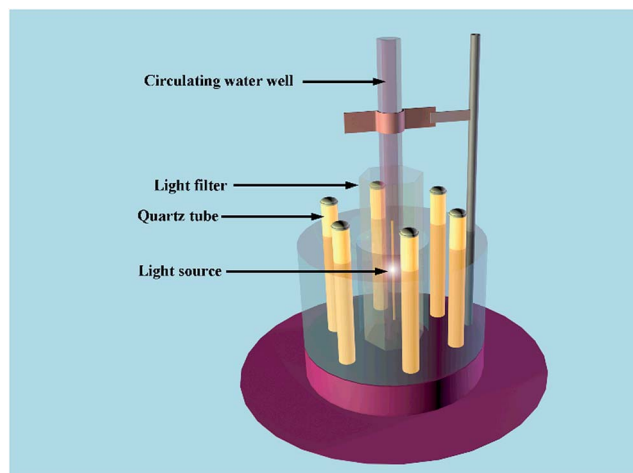


Fig. 1 Rotary photochemical reactor with a 350 W xenon lamp and 420 nm cut-off filter.

Photocatalytic experiments

Photocatalytic activity tests of the photocatalysts were carried out in a XPA-7 rotary photochemical reactor (Fig. 1, Nanjing Xujiang machine plant). A 350 W xenon lamp with a 420 nm cut-off filter was used as the visible-light irradiation source. For each experiment, 50 mL of a 4 mg L⁻¹ ENX aqueous solution with 1.0 g L⁻¹ catalysts was introduced into a 50 mL quartz tube, which was adjusted to a neutral pH *via* 1% NaOH and H₂SO₄ solution. Before the light irradiation, the reaction solution was stirred in the dark for 30 min to reach adsorption equilibrium for ENX on the photocatalyst. The samples were filtered through 0.22 μm millipore filters to remove the nanophotocatalyst. ENX was analyzed by high-performance liquid chromatography (HPLC), and the chromatographic conditions of ENX are listed as follows: column: Zorbax Eclipse XDB-C18, 4.6 × 150 mm, 5 μm; temperature: 40 °C; mobile phase: methanol/Milli-Q water containing 0.2% formic acid (65 : 25 v/v); flow rates: 1 mL min⁻¹; injection volume: 20 μL; and detection wavelength: 278 nm.

The quenching experiments were employed to prove the existence of reactive species in the ENX photodegradation process. Herein, 0.0001 mol L⁻¹ benzoquinone (BQ, O₂^{•-} scavenger), 0.01 mol L⁻¹ isopropanol (IPA, ·OH scavenger), 0.01 mol L⁻¹ potassium iodide (KI, ·OH and h⁺ scavenger), and 0.075 mol L⁻¹ sodium azide (NaN₃, ¹O₂ scavenger) were used as quenchers in the experiments.^{30–33}

Results and discussion

Characterization

To determine the real contents of g-C₃N₄ in TiO₂/g-C₃N₄, thermogravimetric analysis was performed from 30 °C to 800 °C at a heating rate of 10 °C min⁻¹ under air conditions. It can be observed from Fig. 2 that the burning of g-C₃N₄ occurs in the temperature range of 500–650 °C, and the pure TiO₂ presents almost no weight loss, which is in accordance with the previous

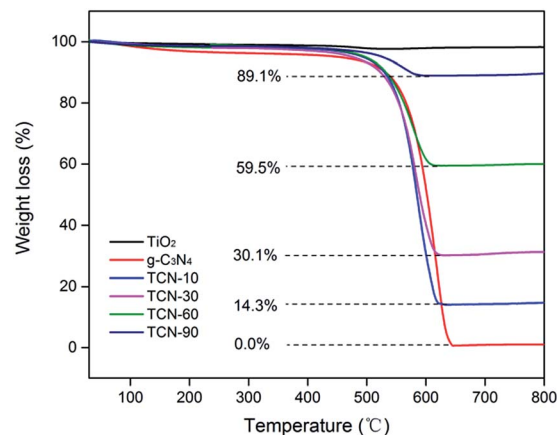


Fig. 2 TG analysis of the as-prepared samples.

report.³⁴ As shown in Fig. 2, the real contents of g-C₃N₄ can be easily calculated from the weight remained after combustion.

Fig. 3 shows the TEM and HRTEM images of the obtained materials. It can be clearly observed that the g-C₃N₄ displays a graphite-like layered structure with the agglomeration of TiO₂ on the surface (Fig. 3A and B). CDs, as the decoration of TiO₂/g-C₃N₄ heterojunction, are embedded in TiO₂ nanoparticles and deposited onto the surface of g-C₃N₄ nanosheets (Fig. 3C and D). The HRTEM images of the CDs/TiO₂/g-C₃N₄ samples (Fig. 3E) clearly reveal an interplanar spacing of 0.35 nm, which authenticates the existence of TiO₂ (anatase 101).³⁵ HRTEM images of CDs and the inset in Fig. 3F show CDs (average size:

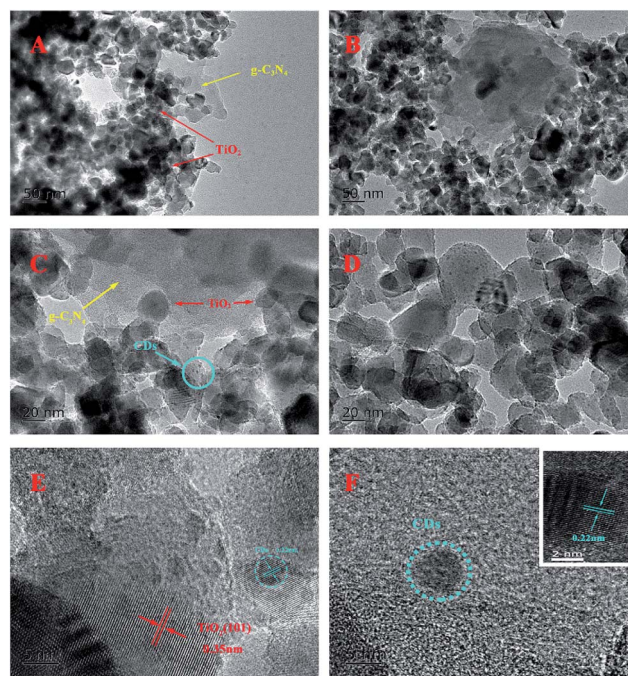


Fig. 3 (A and B) TEM images of TCN-90; (C and D) TEM images of CTCN-1; (E) HRTEM image of CTCN-1; and (F) HRTEM image of CDs. Inset: HRTEM image of CDs with obvious crystal lattice.



~5 nm) with a lattice spacing of 0.22 nm corresponding to the (100) facet of graphite.³⁶

XRD was carried out to reveal the phase composition of the samples (Fig. 4). As shown in Fig. 4A, no impurity diffraction peaks are observed in the XRD patterns of TiO₂ and g-C₃N₄, which can be indexed to anatase (JCPDS 21-1272), rutile phases (JCPDS 21-1276) of TiO₂, and hexagonal phase of g-C₃N₄ (JCPDS 87-1526). TCN-90 samples show relatively strong peaks at the position of R(100), indicating the introduction of g-C₃N₄. After decoration of CDs, the characteristic diffraction peaks of TiO₂/g-C₃N₄ remain unchanged with the increasing mass contents of CDs. It can be concluded that CDs have a negligible effect on the crystalline structure of the TiO₂/g-C₃N₄ Z-scheme, decorated *via* a facile hydrothermal process. For others, no new diffraction peaks appear due to the low doping content of CDs.

To study the surface chemical composition and chemical status of CD/TiO₂/g-C₃N₄, XPS analysis was carried out, and the results are shown in Fig. 5. It can be concluded that the ternary composites primarily consist of C, N, Ti, and O elements (see Fig. 5A). High-resolution spectra of C 1s at 288.88 eV and 284.78 eV are shown in Fig. 5B. The former can be attributed to the N-C=N bonds, whereas the latter is assigned to the C-C coordination including sp²-hybridized C atoms present in g-C₃N₄.³⁷ High-resolution spectra of C 1s of TCN-90 are provided as a contrast. It can be observed that C-C at 288.88 eV of CTCN-1 occupies relatively larger percentage than TCN-90 due to the doping of CDs. The N 1s high-resolution spectrum in Fig. 5C shows three individual peaks with the binding energies of 400.98 eV, 399.98 eV, and 398.78 eV, which can correspond to C-N-H, N-(C)₃, and C=N-C, respectively.³⁸ From Fig. 5D, due to the phenomena of spin-orbit separation, two peaks at the binding energies of 458.88 eV (Ti 2p_{3/2}) and 464.58 eV (Ti 2p_{1/2}) suggest the existence of Ti⁴⁺ in the composite.³⁹ The O 1s high-resolution spectrum in Fig. 5E is observed at the binding energies of 532.08 eV and 530.48 eV, which are ascribed to the O-H bond and Ti-O bond, respectively.^{40,41} The former can be connected to the presence of a hydroxyl group on the surface of the CDs/TiO₂/g-C₃N₄ composite, which is in line with the FT-IR analysis in Fig. 6.

The FT-IR spectra of the TiO₂ microspheres, g-C₃N₄, TCN-90 composite, and CTCN-1 composite are shown in Fig. 6. For TiO₂, a wide absorption band can be observed at 500–700 cm⁻¹, which is attributed to Ti-O stretching.⁴² The peaks at 1640 cm⁻¹ and 3420 cm⁻¹ are related to the bending vibration of O-H and

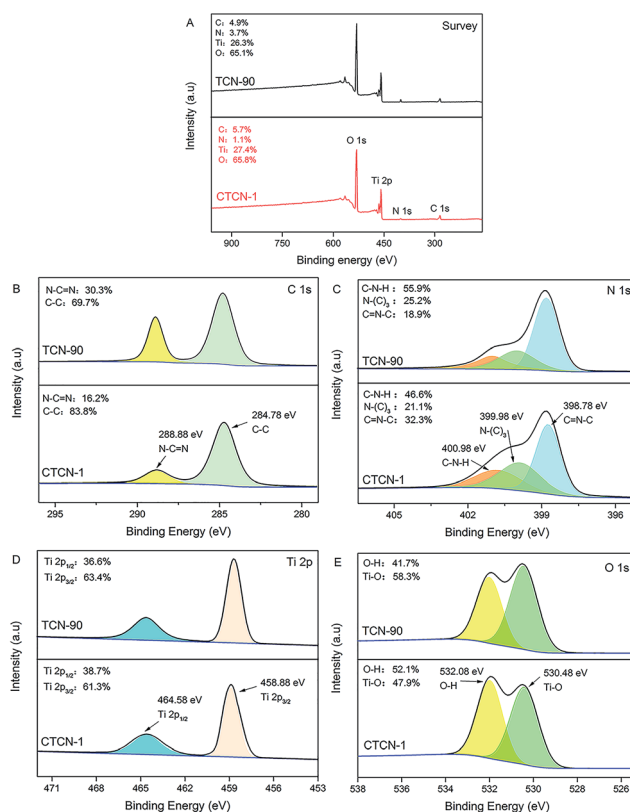


Fig. 5 X-ray photoelectron spectra (XPS) survey spectrum of CTCN-1 and TCN-90 (A); high-resolution spectra of the C 1s (B), N 1s (C), Ti 2p (D), and O 1s (E) of CTCN-1 and TCN-90.

N-H.⁴³ For g-C₃N₄, the peak at 1630 cm⁻¹ corresponds to the C-N heterocycle stretching vibration modes, whereas the peaks at 1450 cm⁻¹ and 1250 cm⁻¹ can be assigned to aromatic C-N stretching vibration modes.⁹ The peaks at 808 cm⁻¹ and 3170 cm⁻¹ are in accordance with the characteristic breathing mode of triazine units and N-H.¹⁵ A peak at 1409 cm⁻¹ is observed in the FTIR spectra of both TCN-90 and CTCN-1, which can be interpreted as the introduction of g-C₃N₄ and CDs.

The optical properties of the as-prepared samples were characterized by the DRS technique, and the results are shown in Fig. 7A. TiO₂ and g-C₃N₄ each revealed a basal absorption

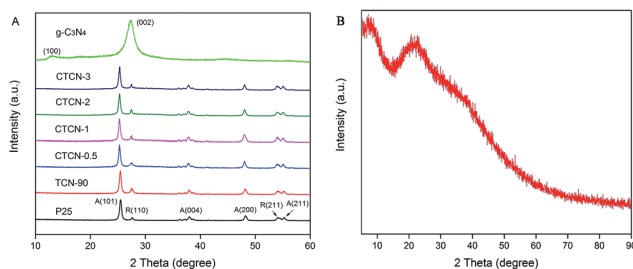


Fig. 4 (A) XRD patterns of TiO₂, g-C₃N₄, TCN-90, CTCN-0.5, CTCN-1, CTCN-2, and CTCN-3; (B) XRD patterns of CDs.

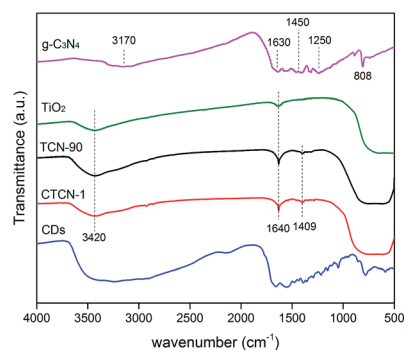


Fig. 6 FT-IR spectra of the as-prepared samples.



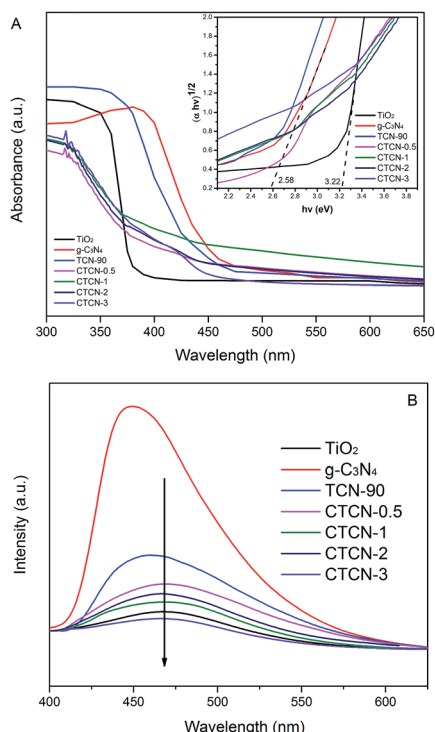


Fig. 7 UV-vis diffuse reflectance spectra. Inset: band gap of the as-prepared photocatalyst determined from the $(\alpha hv)^{1/2}$ versus photon-energy (A) and photoluminescence spectra under 350 nm excitation (B) of the photocatalysts.

band at ~ 390 nm and ~ 475 nm, respectively, which was consistent with previous reports.^{31,44,45} $g\text{-C}_3\text{N}_4/\text{TiO}_2$ possesses the absorption features of single TiO_2 and $g\text{-C}_3\text{N}_4$, which indicates the existence of $g\text{-C}_3\text{N}_4$. As expected, $\text{CD}/\text{TiO}_2/g\text{-C}_3\text{N}_4$ shows obvious additional absorption in the 370–450 nm region when doped with different amounts of CDs. The absorption edge of CTCN-1 ternary composite shows a remarkable red shift towards a higher wavelength at ~ 450 nm; this suggests that the ternary composite is able to utilize the visible-light region better. Herein, Kubelka–Munk transformation was used to estimate the band gap energies of the semiconductors according to eqn (1).

$$(\alpha hv)^{(1/2)} = A(hv - E_g) \quad (1)$$

where α is the absorption coefficient, ν is the light frequency, E_g is the band gap energy, and A is a constant.⁴⁶ The potentials of VB and CB of the catalyst can be estimated according to eqn (2) and (3), respectively.

$$E_{\text{VB}} = X - E_c + 0.5E_g \quad (2)$$

$$E_{\text{CB}} = E_{\text{VB}} - E_g \quad (3)$$

where X is the electronegativity of the semiconductor (X values are 5.81 eV for TiO_2 and 4.72 eV for $g\text{-C}_3\text{N}_4$) and E_c is the energy of free electrons on the hydrogen scale (about 4.5 eV). The energy band structure parameters are listed in Table S1.†

PL spectra were obtained (Fig. 7B) to detect the recombination of electron–hole pairs. Generally, lower PL intensity corresponds to lower recombination of electron–hole pairs, contributing to higher photocatalytic activity.⁴⁷ The $g\text{-C}_3\text{N}_4$ has an intensive emission peak at around 460 nm, which can be attributed to the fast recombination of the photoinduced electron–hole pairs of $g\text{-C}_3\text{N}_4$. The intensities of the peaks for CTCN-0.5, CTCN-1, CTCN-2, and CTCN-3 are much lower than those for TCN-90, revealing that CDs conduce to slow the recombination rate of electron–hole pairs. Further, the emission peak of $\text{CDs}/\text{TiO}_2/g\text{-C}_3\text{N}_4$ shows an obvious red-shift from 455 nm to 470 nm after doping of CDs, which demonstrates the existence of CDs from another perspective. The PL results confirm the importance of $\text{CDs}/\text{TiO}_2/g\text{-C}_3\text{N}_4$ in blocking the recombination of electrons and holes.

PL spectra of CDs are shown in Fig. 8, which demonstrate superior up-converted photoluminescence property of CDs. When CDs were excited by long-wavelength light (from 600 nm to 900 nm), the up-converted emissions were significantly located in the range from 350 nm to 600 nm. These results imply that CDs might enhance the photocatalytic efficiency *via* the conversion of near-infrared wavelength to visible light, which markedly promotes the light utilization of the photocatalysts.

Photocatalytic performance of composites

Fig. 9 displays the photocatalytic degradation of ENX over various photocatalysts. As can be seen, the self-photolysis of ENX could be neglected in the blank experiment. For TCN-90 (see Fig. 9A), the concentration of ENX is reduced to 45.95% in 1 h. This means TCN-90 performs better than other doping ratios of $g\text{-C}_3\text{N}_4$, which confirms that the small doping ratio of $g\text{-C}_3\text{N}_4$ is in favour of ENX degradation. After doping of CDs (1 wt%), enhanced photocatalytic activity was exhibited by both TiO_2 and $g\text{-C}_3\text{N}_4$, which could be attributed to the up-converted PL property. In Fig. 9B, we drew a comparison between TiO_2 , TiO_2/CDs , $g\text{-C}_3\text{N}_4$, $g\text{-C}_3\text{N}_4/\text{CDs}$, TCN-90, CTCN-0.5, CTCN-1, CTCN-2, and CTCN-3 in the photocatalytic degradation of ENX. CTCN-1 was found to be the most optimal photocatalyst among all the photocatalysts as it reduced ENX to 8.34% in 1 h,

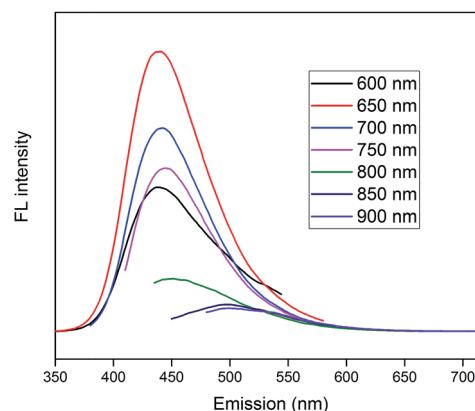


Fig. 8 Up-converted PL spectra of CDs.



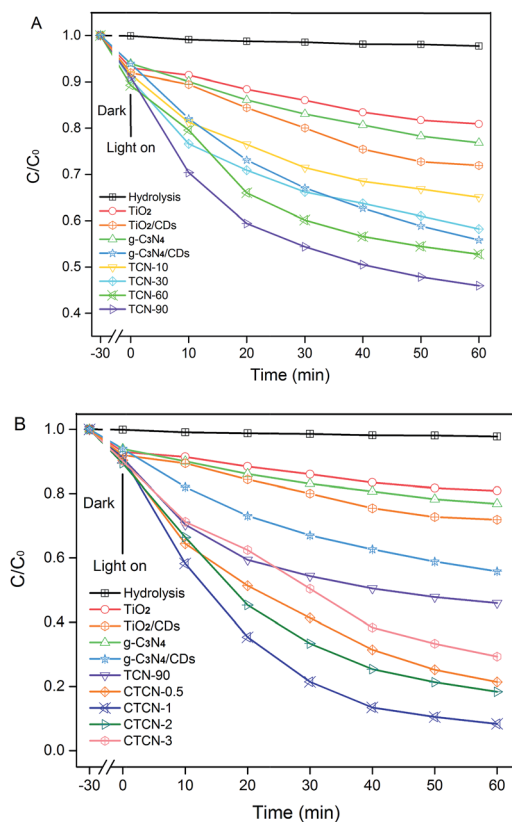


Fig. 9 Photocatalytic activity of $\text{TiO}_2/\text{g-C}_3\text{N}_4$ binaries (A) and CDs/ $\text{TiO}_2/\text{g-C}_3\text{N}_4$ ternaries (B) based on the photocatalytic degradation of ENX under visible-light irradiation ($\lambda > 420$ nm).

which corresponds to the DRS results in Fig. 7A. Compared with the single-component (TiO_2 and $\text{g-C}_3\text{N}_4$) samples and two-component samples (TiO_2/CDs , $\text{g-C}_3\text{N}_4/\text{CDs}$, TCN-90), CD/ $\text{TiO}_2/\text{g-C}_3\text{N}_4$ exhibits remarkably enhanced photocatalytic activity, owing to the introduction of CDs as an electron reservoir and transporter. However, further CD loading (>1.0 wt%) leads to decreased degradation rates, which can be attributed to the inner filter effect of CDs *via* scrambling for the absorption of photons and reduction of the formation of reactive species.⁴⁸

Reusability is a critical factor for practical utilization. To investigate the stability of CD/ $\text{TiO}_2/\text{g-C}_3\text{N}_4$, five photocatalytic experiment cycle runs were completed, and the results are shown in Fig. 10. As a result, 88.7% of the ENX was decomposed in 60 min in the fifth cycle, which was slightly reduced as compared to that in the first round (91.6%). Thus, the CTCN-1 can be identified as a stable photocatalyst.

To study the generation of radicals in the photocatalytic system under visible-light irradiation ($\lambda > 420$ nm), the ESR spin-trap with DMPO technique was used. As shown in Fig. 11, the signals of $\text{O}_2^{\cdot-}$ and $\cdot\text{OH}$ increase with time elapsing in 10 minutes, whereas no signals appear in the dark. The weak signals of $\text{O}_2^{\cdot-}$ and $\cdot\text{OH}$ radicals in TiO_2 can be attributed to fast recombination of photogenerated electron-hole pairs.⁴⁹ Because the VB position of $\text{g-C}_3\text{N}_4$ (+1.36 eV) is more negative than the standard redox potential of $\cdot\text{OH}/\text{OH}^-$ (+1.99 eV) and

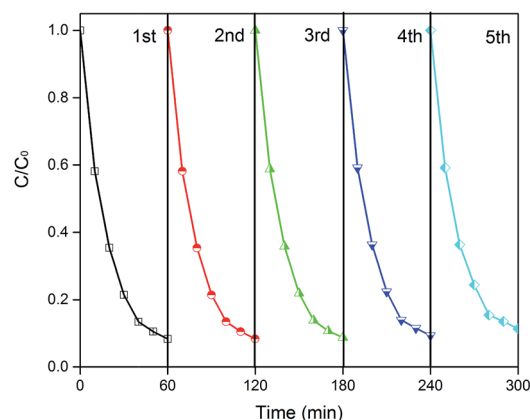


Fig. 10 The repeated photocatalytic experiments for CTCN-1.

$\cdot\text{OH}/\text{H}_2\text{O}$ (+2.73 eV), h^+ of $\text{g-C}_3\text{N}_4$ fails to provide $\cdot\text{OH}$ by oxidizing OH^- or H_2O .⁵⁰ The signals of $\cdot\text{OH}$ radicals appear in $\text{g-C}_3\text{N}_4$ due to the reaction of $\text{O}_2^{\cdot-}$ and h^+ .⁵¹ Compared with TCN-90, the signals of $\text{O}_2^{\cdot-}$ radicals are greatly enhanced for CTCN-1, indicating that CDs play a significant role as electron mediator to improve the photocatalytic activity of CD/ $\text{TiO}_2/\text{g-C}_3\text{N}_4$. Simultaneously, the signals of $\text{O}_2^{\cdot-}$ radicals are also improved, demonstrating the increased photocatalytic activity of CD-modified $\text{TiO}_2/\text{g-C}_3\text{N}_4$.

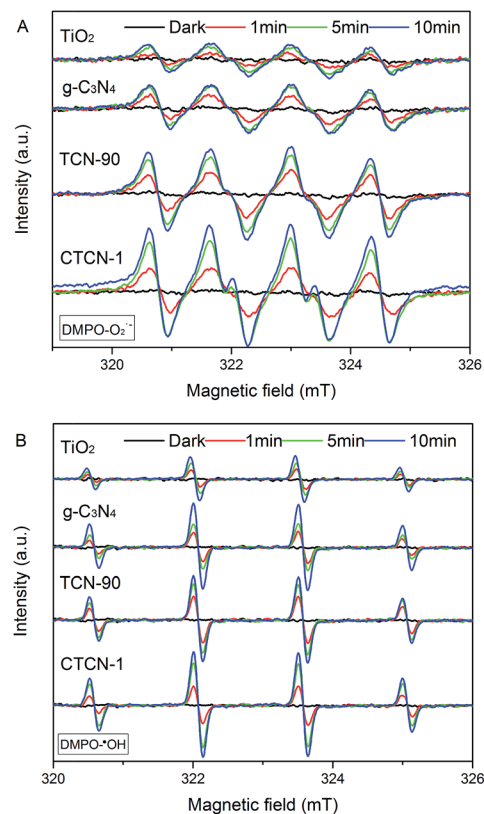


Fig. 11 DMPO spin-trapping ESR spectra under visible-light irradiation ($\lambda > 420$ nm) in aqueous solutions (A) and ethanol solutions (B).



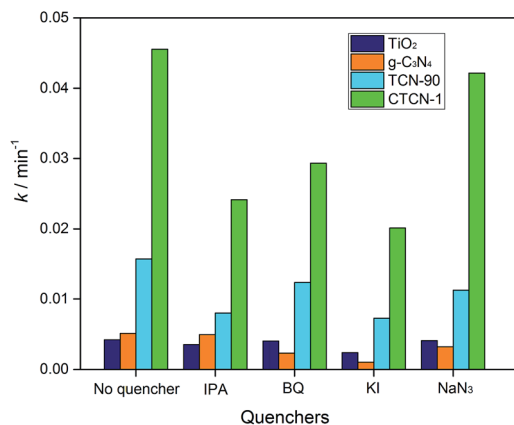


Fig. 12 Kinetic constants of the as-prepared photocatalysts with different quenchers.

Fig. 12 shows the kinetic constants of TiO₂, g-C₃N₄, TCN-90, and CTCN-1 in the presence of different quenchers. For the addition of isopropanol (IPA, ·OH scavenger) and KI (·OH and h⁺ scavenger), a slight decrease can be observed in the degradation of ENX by CTCN-1, indicating the minor role of h⁺. For the TCN-90 composite, similar results were obtained, whereas a slight decrease of *k* was observed after the addition of NaN₃ (¹O₂ scavenger) for the TCN-90 and CTCN-1 composites. Although benzoquinone (BQ, O₂^{·-} scavenger) has a slight effect in the presence of TCN-90, it plays a quite important role in CTCN-1 probably because CDs can act as electron mediators and generate more O₂^{·-}.

Based on the abovementioned results and the previous study,^{43,52–54} the potential photocatalytic mechanisms are proposed in Fig. 13. For the conventional TiO₂/g-C₃N₄ heterojunctions, electron–hole pairs are formed at the *E*_{CB} and *E*_{VB} of TiO₂ and g-C₃N₄ under visible light. Subsequently, h⁺ generates at the *E*_{VB} of TiO₂ and transfers to the *E*_{VB} of g-C₃N₄, and the e⁻ from *E*_{CB} of g-C₃N₄ can transfer to the *E*_{CB} of TiO₂. However, the h⁺ from *E*_{VB} of g-C₃N₄ cannot oxidize OH⁻ or H₂O to generate ·OH because of the negative valence band position of g-C₃N₄.

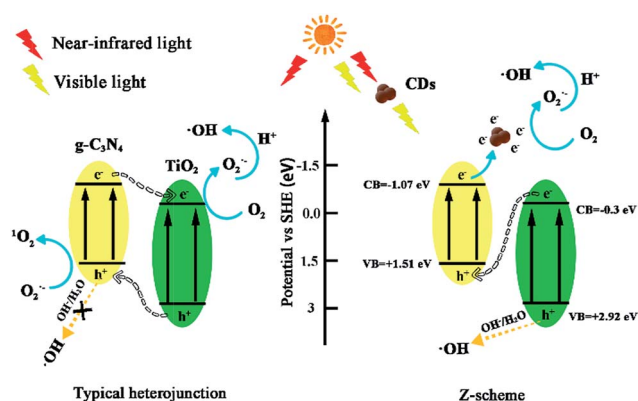


Fig. 13 Photocatalytic mechanism scheme in conventional TiO₂/g-C₃N₄ heterojunctions and TiO₂/g-C₃N₄ Z-scheme with the introduction of CDs.

(+1.51 eV), which is less than the standard redox potential of ·OH/OH⁻ (+1.99 eV) and ·OH/H₂O (+2.73 eV). The e⁻ from TiO₂ may be captured by molecular oxygen to generate O₂^{·-} radicals,⁵⁵ which can directly attack pollutants. If TiO₂/g-C₃N₄ follows this mechanism, h⁺ should play a major role in the photocatalytic system, whereas IPA has minor effects. However, the quenching experiments and ESR spectra results have contradicted this hypothesis. Moreover, the results of the ¹O₂ quenching experiment are inconsistent with this mechanism. Thus, the TiO₂/g-C₃N₄ photocatalyst follows the direct Z-scheme type mechanism.

For the TiO₂/g-C₃N₄ Z-scheme with the introduction of CDs, the near-infrared light wavelength could be converted to visible light due to the up-converted PL properties of CDs.⁵³ Herein, the presence of CDs can facilitate a Z-scheme transfer mechanism, which differs from the general heterostructured mechanism. The general heterostructured mechanism can hardly interpret the formation of ·OH, and the transfer speed of electrons and holes might be very slow.⁵⁶ The active species, h⁺, O₂^{·-}, ¹O₂, and ·OH can effectively degrade ENX into small molecule compounds or directly into final products such as CO₂ and H₂O.

Conclusions

In this study, CDs/TiO₂/g-C₃N₄ was synthesized *via* a facile hydrothermal method, which exhibited high photocatalytic performance towards the degradation of ENX under visible-light irradiation. The results of the characterization verified the formation of CD/TiO₂/g-C₃N₄, in which the CDs were embedded in TiO₂ nanoparticles and deposited onto the surface of the g-C₃N₄ nanosheets. The enhanced photocatalytic performance of CDs/TiO₂/g-C₃N₄ might be attributed to the unique up-converted PL property, efficient charge separation, and efficient electron transportation of CDs. The synergistic effects could be concluded as follows: (1) the extension of visible-light response scope; (2) efficient photogenerated electron–hole pair separation; and (3) retardation of charge recombination. The active species h⁺, O₂^{·-}, ¹O₂, and ·OH were produced in the Z-scheme system. The present study confirms that the CD/TiO₂/g-C₃N₄ catalyst is efficient, stable, and reusable for environmental applications.

Acknowledgements

This work was supported by the National Natural Science Foundation of China (No. 21377031 and 21677040) and the Scientific and Technical Projects of Guangdong Province (No. 2013B020800009).

Notes and references

- 1 S. M. Lam, J. C. Sin and A. R. Mohamed, *Mater. Sci. Semicond. Process.*, 2016, **47**, 62–84.
- 2 O. Mehraj, N. A. Mir, B. M. Pirzada, S. Sabir and M. Muneer, *J. Mol. Catal. A: Chem.*, 2014, **395**, 16–24.



- 3 M. J. Nalbandian, M. Zhang, J. Sanchez, Y. H. Choa, D. M. Cwiertyny and N. V. Myung, *J. Mol. Catal. A: Chem.*, 2015, **404**, 18–26.
- 4 G. W. Cui, W. L. Wang, M. Y. Ma, M. Zhang, X. Y. Xia, F. Y. Han, X. F. Shi, Y. Q. Zhao, Y. B. Dong and B. Tang, *Chem. Commun.*, 2013, **49**, 6415–6417.
- 5 T. H. Tan, J. Scott, H. N. Yun, R. A. Taylor, K. F. Agueyinsou and R. Amal, *ACS Catal.*, 2016, **6**(3), 1870–1879.
- 6 L. Pan, S. Wang, J. Xie, L. Wang, X. Zhang and J. J. Zou, *Nano Energy*, 2016, **28**, 296–303.
- 7 L. Pan, S. Wang, J. J. Zou, Z. F. Huang, L. Wang and X. Zhang, *Chem. Commun.*, 2014, **50**, 988–990.
- 8 X. Wang, K. Maeda, A. Thomas, K. Takanabe, G. Xin, J. M. Carlsson, K. Domen and M. Antonietti, *Nat. Mater.*, 2009, **8**, 76.
- 9 L. Ge, F. Zuo, J. Liu, Q. Ma, C. Wang, D. Sun, L. Bartels and P. Feng, *J. Phys. Chem. C*, 2012, **116**, 13708–13714.
- 10 B. Chai, J. Yan, C. Wang, Z. Ren and Y. Zhu, *Appl. Surf. Sci.*, 2016, **391**, 376–383.
- 11 S. Li, F. Zheng, S. Cai, W. Liang and Y. Li, *Sens. Actuators, B*, 2013, **188**, 280–285.
- 12 D. R. Baker and P. V. Kamat, *Adv. Funct. Mater.*, 2010, **19**, 805–811.
- 13 X. Zhong, M. Jin, H. Dong, L. Liu, L. Wang, H. Yu, S. Leng, G. Zhuang, X. Li and J. G. Wang, *J. Solid State Chem.*, 2014, **220**, 54–59.
- 14 H. Tang, S. Chang, L. Jiang, G. Tang and W. Liang, *Ceram. Int.*, 2016, **42**, 18443–18452.
- 15 M. Reli, P. Huo, M. Šihor, N. Ambrožová, I. Troppová, L. Matějová, J. Lang, L. Svoboda, P. Kuśtrowski and M. Ritz, *J. Phys. Chem. A*, 2016, **120**, 8564–8573.
- 16 X. Xu, Z. Bao, Z. Gang, H. Zeng and J. Hu, *ACS Appl. Mater. Interfaces*, 2016, **8**, 14118–14124.
- 17 Y. Guo, P. Yao, D. Zhu and G. Cheng, *J. Mater. Chem. A*, 2015, **3**, 13189–13192.
- 18 X. Wu, J. Zhao, L. Wang, M. Han, M. Zhang, H. Wang, H. Huang, Y. Liu and Z. Kang, *Appl. Catal., B*, 2017, **206**, 501–509.
- 19 H. Yu, Y. Liang, Y. Rao, D. Zhu, J. Cao, Z. Shen, W. K. Ho and S. C. Lee, *Environ. Sci. Technol.*, 2017, **51**, 2924–2933.
- 20 J. L. Liu and M. H. Wong, *Environ. Int.*, 2013, **59**, 208–224.
- 21 G. R. Boyd, H. Reemtsma, D. A. Grimm and S. Mitra, *Sci. Total Environ.*, 2003, **311**, 135.
- 22 B. J. Richardson, P. K. Lam and M. Martin, *Mar. Pollut. Bull.*, 2005, **50**, 913.
- 23 B. Kasprzykhordern, R. M. Dinsdale and A. J. Guwy, *Water Res.*, 2009, **43**, 363–380.
- 24 R. Shen and S. A. Andrews, *Water Res.*, 2011, **45**, 944–952.
- 25 T. Lin, S. Yu and W. Chen, *Chemosphere*, 2016, **152**, 1.
- 26 J. Radjenović, M. Petrović, F. Ventura and D. Barceló, *Water Res.*, 2008, **42**, 3601–3610.
- 27 S. Qu, X. Wang, Q. Lu, X. Liu and L. Wang, *Angew. Chem., Int. Ed.*, 2012, **51**, 12215–12218.
- 28 F. Dong, L. Wu, Y. Sun, M. Fu, Z. Wu and S. C. Lee, *J. Mater. Chem.*, 2011, **21**, 15171–15174.
- 29 J. Yu, S. Wang, J. Low and W. Xiao, *Phys. Chem. Chem. Phys.*, 2013, **15**, 16883–16890.
- 30 G. Li, X. Nie, J. Chen, Q. Jiang, T. An, P. K. Wong, H. Zhang, H. Zhao and H. Yamashita, *Water Res.*, 2015, **86**, 17.
- 31 H. Xiao, J. Zhu and A. Thomas, *RSC Adv.*, 2015, **5**, 105731–105734.
- 32 G. Li, K. H. Wong, X. Zhang, C. Hu, J. C. Yu, R. C. Chan and P. K. Wong, *Chemosphere*, 2009, **76**, 1185–1191.
- 33 J. Cao, B. Xu, B. Luo, H. Lin and S. Chen, *Appl. Surf. Sci.*, 2011, **257**, 7083–7089.
- 34 Y. He, L. Zhang, X. Wang, Y. Wu, H. Lin, L. Zhao, W. Weng, H. Wan and M. Fan, *RSC Adv.*, 2014, **4**, 13610–13619.
- 35 X. Sun, W. Dai, G. Wu, L. Li, N. Guan and M. Hunger, *Chem. Commun.*, 2015, **51**, 13779.
- 36 X. Zhai, P. Zhang, C. Liu, T. Bai, W. Li, L. Dai and W. Liu, *Chem. Commun.*, 2012, **48**, 7955.
- 37 J. A. Singh, S. H. Overbury, N. J. Dudney, M. Li and G. M. Veith, *ACS Catal.*, 2012, **2**, 1138–1146.
- 38 S. J. Yang, J. H. Cho, G. H. Oh, K. S. Nahm and C. R. Park, *Carbon*, 2009, **47**, 1585–1591.
- 39 X. Yang, J. Qin, J. Yan, K. Chen, X. Yan, Z. Du, L. Rong and T. Hua, *Appl. Catal., B*, 2015, **166–167**, 231–240.
- 40 Y. Chen, W. Huang, D. He, S. Yue and H. Hong, *ACS Appl. Mater. Interfaces*, 2014, **6**, 14405.
- 41 L. A. D. Silva, V. A. Alves, S. C. D. Castro and J. F. C. Boodts, *Colloids Surf., A*, 2000, **170**, 119–126.
- 42 J. Yu, S. Wang, J. Low and W. Xiao, *Phys. Chem. Chem. Phys.*, 2013, **15**, 16883.
- 43 Y. Chen, W. Huang, D. He, Y. Situ and H. Huang, *ACS Appl. Mater. Interfaces*, 2014, **6**, 14405.
- 44 N. Boonprakob, N. Wetchakun, S. Phanichphant, D. Waxler, P. Sherrell, A. Nattestad, J. Chen and B. Inceesungvorn, *J. Colloid Interface Sci.*, 2014, **417**, 402–409.
- 45 Z. F. Huang, J. Song, L. Pan, Z. Wang, X. Zhang, J. J. Zou, W. Mi, X. Zhang and L. Wang, *Nano Energy*, 2015, **12**, 646–656.
- 46 J. Tauc, *Mater. Res. Bull.*, 1970, **5**, 721–729.
- 47 X. Zhou, B. Jin, L. Li, F. Peng, H. Wang, H. Yu and Y. Fang, *J. Mater. Chem.*, 2012, **22**, 17900–17905.
- 48 J. Pan, Y. Sheng, J. Zhang, J. Wei, P. Huang, X. Zhang and B. Feng, *J. Mater. Chem. A*, 2014, **2**, 18082–18086.
- 49 K. Lv, X. Li, K. Deng, J. Sun, X. Li and M. Li, *Appl. Catal., B*, 2010, **95**, 383–392.
- 50 D. Wu, B. Wang, W. Wang, T. An, G. Li, T. W. Ng, H. Y. Yip, C. Xiong, H. K. Lee and P. K. Wong, *J. Mater. Chem. A*, 2015, **3**, 15148–15155.
- 51 J. Ng, X. Wang and D. D. Sun, *Appl. Catal., B*, 2011, **110**, 260–272.
- 52 Y. Li, K. Lv, W. Ho, F. Dong, X. Wu and Y. Xia, *Appl. Catal., B*, 2017, **202**, 611–619.
- 53 F. Wang, P. Chen, Y. Feng, Z. Xie, Y. Liu, Y. Su, Q. Zhang, Y. Wang, K. Yao and W. Lv, *Appl. Catal., B*, 2017, **207**, 103–113.
- 54 Y. He, L. Zhang, M. Fan, X. Wang, M. L. Walbridge, Q. Nong, Y. Wu and L. Zhao, *Sol. Energy Mater. Sol. Cells*, 2015, **137**, 175–184.
- 55 J. Liu, Y. Yang, N. Liu, Y. Liu, H. Huang and Z. Kang, *Green Chem.*, 2014, **16**, 4559–4565.
- 56 Y. He, L. Zhang, B. Teng and M. Fan, *Environ. Sci. Technol.*, 2015, **49**, 649.

